Mater.Phys.Mech.1 (2000) 73-82

HOT WIRE CVD OF HETEROGENEOUS AND POLYCRYSTALLINE SILICON SEMICONDUCTING THIN FILMS FOR APPLICATION IN THIN FILM TRANSISTORS AND SOLAR CELLS

R.E.I. Schropp, B. Stannowski, A.M. Brockhoff,
P.A.T.T. van Veenendaal and J.K. Rath

Utrecht University, Debye Institute, P.O. Box 80,000, 3508 TA Utrecht, The Netherlands

Received: June 7, 2000

Abstract. Using Hot Wire Chemical Vapor Deposition (HWCVD), also known as thermocatalytic decomposition, heterogeneous silicon thin films can be obtained with a widely varying degree of order and crystallinity. Specific parameter regimes have been identified which allow the deposition of films with a structure ranging from purely amorphous to fully polycrystalline. In polycrystalline Si, all hydrogen appears in isolated, compact monohydride bonds. A comparison of XTEM and Raman studies confirmed that the 2000 cm^{-1} infrared mode indeed originates from a completely crystalline region and that there is no amorphous tissue in these films. The 2000 cm^{-1} vibration is due to Si-H bonds at completely coalescent crystal faces (between adjacent crystals). In films with this type of crystallinity, oxygen incorporation is greatly reduced, both during growth and after completion. The heterogeneous growth has been utilized in two types of devices, thin film transistors (TFTs) and thin film solar cells. TFTs have been made exhibiting excellent stability. The field-effect channel of these transistors consists of amorphous silicon hosting nanocrystalline domains which yields TFTs with a high mobility of 1.5 $cm^2V^{-1}s^{-1}$, virtually without the usual threshold voltage instabilities. Solar cells with an intrinsic poly-Si absorber layer have also been further optimized by deliberately profiling the active layer. A stepwise profiling sequence has been developed, starting from immediate-nucleation growth of small random crystallites to continued singly oriented growth of columnar polycrystalline material at a deposition rate of 5 Å/s. These *n-i-p* solar cells on stainless steel substrates presently have 4.41 % conversion efficiency. The short circuit current density is as high as 19.95 mA/cm^2 while the light absorbing *i*-layer is only 1.2 μm thick and no enhanced back reflector is used.

1. INTRODUCTION

The method of catalytic decomposition (Catalytic Chemical Vapor Deposition (Cat-CVD;[1])) of silane or silane/hydrogen mixtures at a resistively heated filament (therefore also called Hot Wire Chemical Vapor Deposition (HWCVD; [2])) is becoming increasingly mature [3,4] and presently yields devices with state-of-the-art properties. The silicon films have large potential in low cost photovoltaic devices (solar cells) and thin film transistors (TFTs).

Hot-Wire CVD was first introduced and patented in 1979 as thermal CVD [5]. The technique was further studied by Doyle *et al* [6] and Matsumura [7,8] showing a high deposition rate as the prominent feature.

Renewed interest in the deposition method is due to Mahan *et al* [2,9] who demonstrated for the first time the possibility to produce device-quality *a*-Si:H with a hydrogen concentration below 1 at. %. The principle of the success of HWCVD in obtaining these exceptionally good films is that the feedstock gases are very efficiently cracked into atomic radicals at the surface of the hot filament (usually tungsten or tantalum) if this is kept at a temperature significantly higher than 1500 °C. The reactive species are transported to the substrates in a low pressure ambient which enables a high deposition rate without gas-phase particle formation. Typically high quality amorphous silicon films can be deposited at a rate between 10 and 50 Å/s and micro- or polycrystalline silicon films at a rate between 5 and 10 Å/s.

In this paper we will describe the structural and optoelectronic properties of silicon thin films with varying degree of order. It will be shown that even amorphous-like films possess features that indicate

Corresponding author: R.E.I. Schropp, e-mail: r.e.i.schropp@phys.uu.nl

© 2000 Advanced Study Center Co. Ltd.

order on a nanoscale, whereas films with very compact polycrystallinity can be deposited comprising μm-sized grains in the growth direction.

2. EXPERIMENTAL DETAILS

2.1. Deposition equipment and process parameters.

The HWCVD chamber is connected to a multichamber ultrahigh vacuum (UHV) system, called PASTA [10]. The chamber is equipped with a shutter which, when inserted, shields the substrate from any deposition during preheating.

The substrates can be heated to a maximum temperature of 550 °C by heater elements outside the vacuum in a heater well. The most frequently used temperatures are in the 350 °C – 520 °C range. The wire used as the hot filament is made of tungsten and has a thickness of 0.5 mm. The wire is resistively heated by a dc current and its temperature is kept between 1750 °C and 1950 °C.

Typical deposition conditions are listed for amorphous films and two types of polycrystalline films in Table 1.

Amorphous silicon is typically obtained from pure silane at low pressure, 0.01 – 0.02 mbar. We found that the electronic properties could be improved by moderate dilution with hydrogen (in a SiH_4/H_2 ratio of 2), leaving structural properties unaffected. Silicon films with varying degree of microcrystallinity are obtained at a higher pressure of 0.1 mbar. We distinguish two main types of polycrystalline silicon thin films, one with random oriented small grains (which will be denoted as *Poly1)* and one with columnar, exclusively (220) oriented grains (denoted as *Poly2). Poly1-type* films are obtained from strongly H_2-diluted silane which yields early nucleation at a relatively low deposition rate (≈1 Å/s). Polycrystalline films with a very strong (220) orientation *(Poly2*-type) can be obtained either from pure silane or from silane/hydrogen mixtures (at a moderate SiH_4/H_2 ratio down to 0.1), depending on the temperature of the filament and the process pressure. These polycrystalline films are most interesting, as they have an SiH stretching vibration mode only at 2000 cm^{-1}. They can only be obtained in a carefully controlled deposition regime, which is, obviously, dependent on the geometry of the chamber and even on the pumping system.

2.2 Materials Characterization

We employed a wide scope of characterization methods in order to achieve a comprehensive overview of the film properties as a function of the critical deposition parameters [3]. The electronic defect density was determined from Electron Spin Resonance (ESR). The spectrally resolved optical absorption was obtained from reflection and transmission measurements. The hydrogen content and bonding structure was determined from Fourier Transform InfraRed (FTIR) spectrocopy.

In the case of poly-Si:H, the orientation and size of the crystallites was detected by X-ray diffraction (XRD); the crystalline volume fraction was derived from Raman spectroscopy measurements. The distribution of grain sizes and their structure was investigated by cross sectional Transmission Electron Microscopy (TEM). A detailed characterization of the impurity profiles, primarily tungsten and oxygen, was performed by Secondary Ion Mass Spectroscopy (SIMS) analysis.

2.3 Poly-Si thin films

Hydrogen at crystal boundaries.

Knowledge of hydrogen bonding and transport in the polycrystalline network is essential for understanding the microstructure and grain boundary properties. Moreover, metastabilities (both light induced [11] as well as thermal [12]) have been attributed to hydrogen. In amorphous silicon, the incorporated hydrogen concentration, which depends on the growth temperature and the deposition process, determines the distribution of hydrogen at various sites such as isolated sites, voids or even bubbles [13]. At present, it is not known whether a similar distribution can be expected in poly-Si. Moreover, in poly-silicon, hydrogen is assumed to be predominantly accommodated in the grain boundary region rather than in the interior of the crystals owing to the low solubility limit of the crystalline lattice. However, the interpretation of the hydrogen bonding

Table 1. Deposition conditions used for hot-wire deposition of amorphous and polycrystalline intrinsic silicon films.

Parameter	*a*-Si:H	poly-Si:H (*Poly2*)	poly-Si:H (*Poly1*)
Wire temperature (°C)	1900	1800	1800
Substrate temperature (°C)	430	510	510
SiH_4 flow (sccm)	60	10	1
H_2 flow (sccm)	30	100	100
Process pressure (mbar)	0.02	0.1	0.1
Deposition rate (Å/s)	18	5.5	1

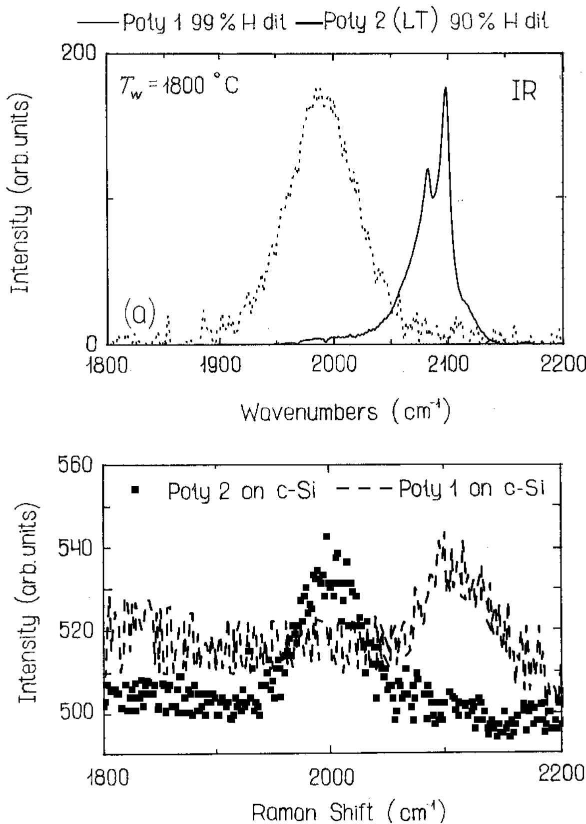

Fig. 1. (a) Infrared absorption spectra and (b) Raman spectra of poly-Si films *Poly1* and *Poly2*.

configuration in poly-Si is still ambiguous. The microscopic structure of the grain boundaries is affected by the long-range order that is imposed on it by the adjacent crystallites.

The hydrogen bonding configuration in device-quality poly-Si, as deposited by HWCVD, appears to be signicantly different from that in micro- or polycrystalline films made by PECVD. The unique optoelectronic properties [14] can be attributed to this structure. Most important is the observation of the stretching mode vibration at 2000 cm^{-1} in our HWCVD poly-Si films made in a controlled regime, instead of at 2100 cm^{-1} commonly reported in the literature for microcrystalline films. By changing the hydrogen dilution in the source gas mixture a range of Si-H stretching vibrations are obtained in HWCVD poly-Si films. For films deposited with low hydrogen dilution (90 %), *Poly2,* the vibration is exclusively at 2000 cm^{-1}, whereas for those made with high hydrogen dilution (99 %), *Poly1,* it is exclusively at 2100 cm^{-1} [14]. Using other deposition conditions [15], both 2000 cm^{-1} and 2100 cm^{-1} modes are observed. The 2100 cm^{-1} vibration is attributed to hydrogen on the surfaces of crystalline grains, commonly observed in the case of PECVD poly-Si films [16]. However, the presence of the Si-H vibration exclusively at 2000 cm^{-1} in the *Poly2* has not been explained in the literature. The origin of this unique hydrogen bonding configuration is addressed below.

Poly-Si films were deposited from hydrogen dilution of silane gas by the HWCVD process. The process pressure (p) is kept at an optimum value of 0.1 mbar. Si-H vibration spectra are found to be sensitive to the deposition conditions, namely hydrogen dilution and wire temperature (T_{wire}). In addition to the films listed in Table 1, *Poly2* films have been made at a range of wire temperatures. Specifically, we distinguish here a low T_{wire} type and a high T_{wire} type, respectively, *Poly2(LT)* made at a T_{wire} of 1800 °C and *Poly2(HT)* made at T_{wire} of 1900 °C. In the remainder of this paper the *Poly2(LT)* films will be labeled for short as *Poly2* since the low T_{wire} is our standard condition. Fig. 1 shows the IR spectra of two types of films; *Poly1*, which has vibration only at 2100 cm^{-1} and *Poly2,* which has vibration only at 2000 cm^{-1}. Fig. 2 shows the Raman spectra of the same poly-Si films when the probe laser light is incident from the top side of the film. Here, also *Poly1* shows the vibration peak at 2100 cm^{-1} and *Poly2* shows the peak at 2000 cm^{-1}. It should be noted that IR transmission probes the property of the whole bulk, whereas Raman spectroscopy probes only a thin layer (penetration depth of the 5145 Å laser line is ≈100 nm in poly-Si). The vibration peaks from Raman and IR are similar for *Poly1* and *Poly2* respectively, suggesting that the structure is homogeneous for both types of films. However, for *Poly1* there is a microscopic difference, i.e., the IR peak is a doublet whereas the Raman peak is a single line. In Fig. 2a, the IR spectrum of *Poly2(HT)* has peaks both at 2000 cm^{-1} and 2100 cm^{-1} (doublet). The surprising result is that for *Poly2(HT),* the Raman spectrum (Fig. 2b) does not detect any vibration at 2100 cm^{-1} as observed in IR. In fact, the Raman peak is very similar to that in *Poly2*, suggesting that the top layer of *Poly2(HT)* and *Poly2* grow in the same way. As the TO peak in the Raman spectrum of both *Poly2* and *Poly2(HT)* shows completely crystalline character (520 cm^{-1}) without any amorphous contribution, we attribute the 2000 cm^{-1} peak to Si-H bonds in a completely crystalline region.

An important observation is that a layer made at *Poly2* condition but with a large air leak in the deposition chamber (high oxygen ambient) shows negligible oxygen incorporation. This confirms that the *Poly2* type of material structure inhibits oxygen incorporation at all circumstances (both during deposition as well as post deposition). The difference in oxygen penetration between *Poly1* and *Poly2* type of films is due to the difference in the structure of these films. It is surprising that the sample *Poly2(HT),* which has a large concentration of grain boundary defects, (Si-H bonds at grain boundaries, 2100 cm^{-1} mode of vibration) also

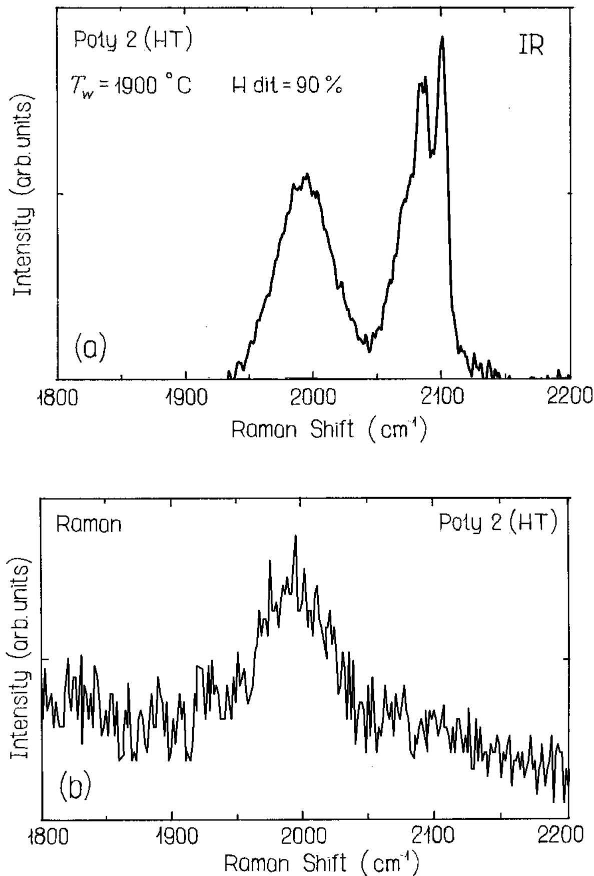

Fig. 2. (a) Infrared spectra and (b) Raman spectra of *Poly2(HT)* films.

shows very little oxygen incorporation. This confirms that the top region of the layers *Poly2* and *Poly2(HT)* have structures of similar compactness. The grain boundary defects buried below this compact layer are isolated from ambient moisture and are unable to pick up the oxygen. The thermal annealing characteristics of *Poly2(HT)* and *Poly2* are similar. They show no change of electrical conductivity upon exposure to air, unlike the *Poly1* film, which showed a metastable increase in conductivity (when exposed to air) that is reversible with annealing.

The interpretation of the splitting of the 2100 cm^{-1} peak (doublet) (see Fig. 2a) is still controversial; many configurations have been proposed such as (1) Si-H bonds on different grain surfaces, i.e., (111) and (100) [15-18], (2) different bonding configurations (monohydride S-H or poly-hydride Si-H_x) [16], (3) optically anisotropic Si-H monolayers residing on grain boundaries [19]. For this *Poly1* film the microscopic difference between IR (splitted) and Raman (single) peaks suggest microscopic changes in the structure during growth, i.e., changes in the hydrogen bonding configuration and grain boundary surfaces or change from "void like (isolated voids, splitted peak)" to "particle like (interconnected voids, single peak)" [19] with increasing thickness. On the other hand, in the *Poly2(HT)* films, the Si-H bonds on the crystal cone surface is at the interface with an amorphous silicon phase. The fact that the IR spectrum of these bonds is also at 2100 cm^{-1} (doublet) suggests that the flexibility of the amorphous network allows the Si-H bond to retain its configuration as in case of Si-H bonds on an open grain surface (as in contact with voids in *Poly1).* However, when the crystal cones coalesce with each other, the Si-H bonds no longer retain the configuration of the open surface, rather are constrained by the symmetry of the adjoining crystal columns. This explains the existence of both the frequencies in IR spectrum of *Poly2(HT).* The Raman spectrum essentially detects this Si-H bond in the top region at 2000 cm^{-1}. For the low T_{wire} film, the Si-H bonds are between closely packed crystal columns throughout the thickness of the films due to which all the Si-H bonds have vibration at 2000 cm^{-1}, which explains why, for *Poly2,* IR (bulk) and Raman (top region) have similar stretching mode characteristics. We attribute the Si-H vibration at 2000 cm^{-1} in our HWCVD poly-Si films to the hydrogen at compact sites which, in addition to the XTEM in defocused conditions, is also confirmed by hydrogen effusion and deuterium diffusion experiments [20]. The matrix between the crystal columns is a strained network constrained by the lattice orientations of the adjoining columns. This strained thin grain boundary region mimics an amorphous network and the Si-H bond inside this compact region resembles the Si-H bond at compact site of *a*-Si:H. Hydrogen evolution experiments give evidence in support of this structure. The hydrogen evolution for *Poly2(HT)* shows a single peak at 650 °C even though it has IR vibration peak at 2100 cm^{-1}. There are no low temperature effusion peaks (due to effusion at inter-connected voids) which are typically observed in microcrystalline films as for example *Poly1.* We infer that the hydrogen effusion through the voids or grain boundaries (2100 cm^{-1} vibration) is limited by the hydrogen diffusion at the compact sites in the top layer.

Oxygen incorporation.

Oxygen contamination of deposited poly-Si films is frequently observed and highly undesirable since oxygen is an *n*-type dopant and leads to traps that reduce the carrier lifetime. Even if the films are deposited in an ultraclean UHV system, in some occasions oxygen can still be present throughout the film. This is a result of post oxidation, which occurs when the film has a porous nature, i.e. if voids form an interconnected substructure through which water vapor can penetrate.

Films made at a high hydrogen dilution of 99 % *(Poly1)* have poor electronic properties and a high ESR defect density of $2.9 \cdot 10^{18}$ cm^{-3}. The high defect density is due to the interconnected void structure, leading to adsorption of moisture from air. Indeed, the oxygen homogeneously penetrates the film to a level of $2 \cdot 10^{21}$ cm^{-3} (measured by SIMS) within a few days of exposure to air, and the ratio of hydrogen to oxygen in the film in the end is in fact 2:1 (as in H_2O). The oxygen is also clearly detected in IR spectra by means of the Si-O band at 1050 cm^{-1} (see Fig. 3). However, an advantage of these films is that they show very good initial nucleation of crystals.

On the other hand, films made at a low hydrogen dilution of 90 % *(Poly2)* have a low ESR defect density of $7.8 \cdot 10^{16}$ cm^{-3}. This is correlated with a low SIMS oxygen concentration of $5 \cdot 10^{18}$ cm^{-3}, a bulk value that is comparable to the oxygen content in *c*-Si as grown by the Czochralski technique and also to that of a pure microcrystalline film deposited by VHF CVD at low deposition rate using an additional gas purifier [21]. Therefore, in *Poly2* material, also no IR signal due to Si-O bonds can be found. Furthermore, as is shown in Fig. 3, also stepwise deposited films (*Poly2* on top of *Poly1)* do not show any Si-O band, demonstrating that *Poly2* is an effective capping layer that protects a porous layer from post oxidation. The effectiveness in shielding from water vapor is due to the compact nature of the *Poly2* material. This compact nature is also characterized by the stretching mode vibration of the monohydride Si-H bonds, which appears at 2000 cm^{-1}, rather than 2100 cm^{-1}, and the fact that hydrogen evolution only takes place at high temperature ($\approx$ 600 °C). This is further elucidated in a forthcoming publication [22].

Poly2 consists of closely connected columnar grains with (220) orientations. However, usually the deposition conditions for *Poly2* material include an initial "incubations"-type growth of amorphous tissue over about 50 nm [23]. Thus, such a profiled *Poly1 / Poly2* structure combines the fast nucleation of *Poly1* with the effective capping property and resistance against oxidation of *Poly2*, such that the whole structure is without amorphous tissue and has very low levels of oxygen.

A cross sectional transmission electron microscope (XTEM) image of a typical profiled layer is shown in Fig. 4. In this micrograph the objective lens was deliberately used in an underfocused position, in order to highlight the void structure. More detailed information is in print in [24]. The *Poly1* part of the film contains elongated, interconnected voids, whereas the *Poly2* section possesses a much lower void fraction, while

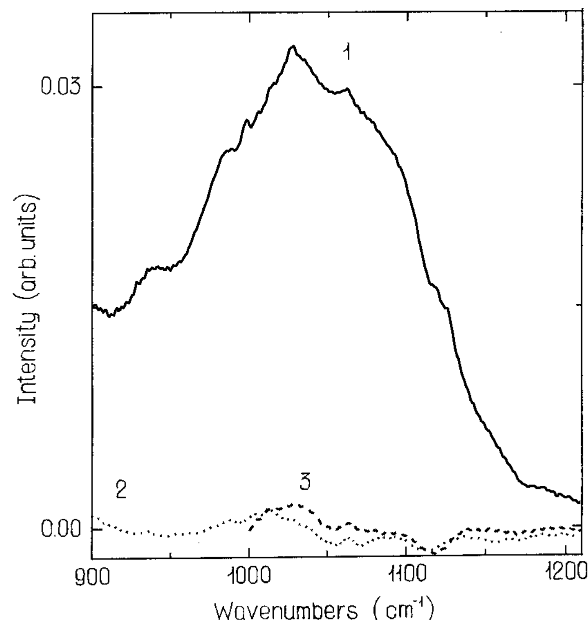

Fig. 3. Infrared absorption spectra of various poly-Si films and double layers, in the regime of the Si-O band. 1 — *Poly1* 550 nm, 2 — *Poly1* 55nm/*Poly2* 1005 nm, 3 — *Poly1* 380 nm/*Poly2* 1070 nm.

the voids are all isolated, thus preventing any oxidation at the grain boundaries.

3. APPLICATION OF HW-DEPOSITED SILICON IN DEVICES

3.1. Thin Film Transistors

The application of Hot-Wire deposited silicon in devices is rather new. For instance, only a few papers [25-27] report on the successful incorporation of this material as the active layer in thin film transistors (TFTs).

We fabricated inverted-staggered TFTs incorporating HWCVD *a*-Si:H and poly-Si:H layers. The basic substrates used were 0.010-0.018 Ωcm *n*-type or *p*-type <100> single crystal silicon wafers that were thermally oxidized. This oxide serves as the gate insulator. Recently, also PECVD silicon nitride (*a*-SiN_x) was used as the gate insulator, thus showing that Hot Wire deposited layers can be compatible with plasma-deposited layers and that it is feasible to produce TFTs incorporating Hot-Wire deposited material also on glass substrates, leading to practical applications.

When TFTs were fabricated on *c*-Si wafers, the oxide at the back side was stripped off. The thickness of the gate insulator amounted to 160-200 nm.

For TFTs made on silicon nitride, the SiN_x was made in a chamber of the ASTER multichamber system from ammonia and silane at a gas flow ratio of NH_3/SiH_4=30, at a substrate temperature of 400 °C, an

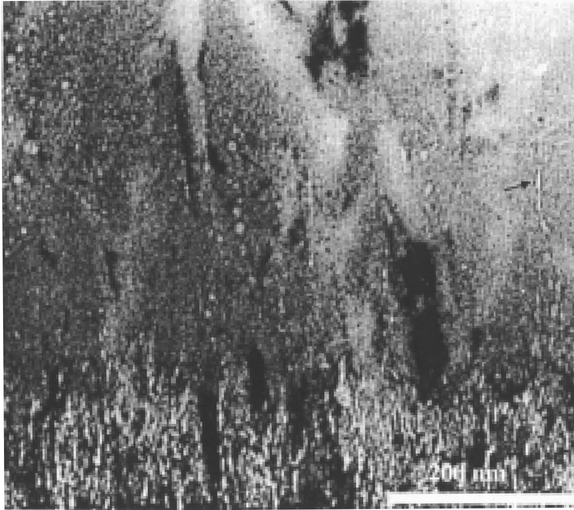

Fig. 4. Cross section micrograph of a *Poly2*-type layer deposited on top of a *Poly1*-type layer.

excitation frequency of 50 MHz, a discharge power density of 225 mW/cm^2, and a pressure of 30 Pa.

The TFTs were analyzed in the dark under ambient conditions with a Hewlett Packard 4156A Parameter Analyzer and a Keithley 283 High-Current Source-Measure Unit. All transfer characteristics were measured with the gate voltage V_g ramped from -5 V to +20 V and with a low source-drain voltage V_s = 0.2 - 0.5 V at all times. The mobility μ_{FE} and the threshold voltage V_t were determined from the current-voltage characteristics in the linear regime, i.e., at low V_s.

HW deposited a-Si:H TFTs.

In Fig. 5 we plotted the transfer characteristics of the *a*-Si:H TFTs. Samples A and B are TFTs comprising HW-deposited *a*-Si:H layers on SiN_x and SiO_2, respectively, and sample C is a reference all-PECVD TFT with SiN_x as the gate insulator. They all show ON-OFF switching ratios higher than 10^5. The field-effect mobilities in the linear regime are 0.74 cm^{2}V^{-1}s^{-1} and 0.66 cm^{2}V^{-1}s^{-1} for the two HW TFTs A and B, respectively, comparable to the mobility of 0.89 cm^{2}V^{-1}s^{-1} for the reference TFT. It should be noted that the reference TFT did not have to be exposed to air (made in a single multichamber system), which may be the reason for the better mobility. As is commonly observed, the threshold voltage for "oxide"-TFTs is higher than for "nitride"-TFTs.

HW deposited poly-Si:H TFTs

For applications of TFTs other than as pixel switching elements in active matrixes, eg. in driver circuitry, it is desirable to have stable characteristics and a carrier mobility that is 1-2 orders of magnitude higher. Poly-Si TFTs can be used to meet these requirements. How-

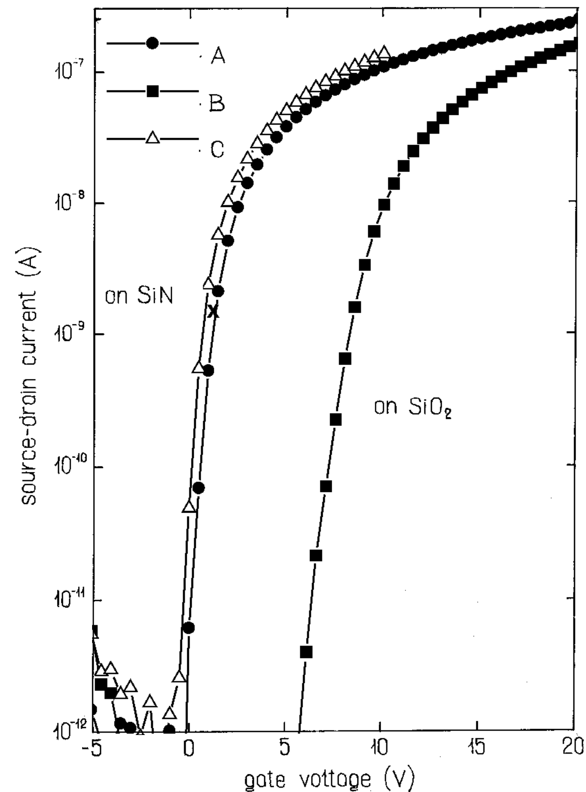

Fig. 5. Linear regime transfer characteristics of *a*-Si:H TFTs. Curve A and B are for TFTs comprising HW-deposited *a*-Si:H layers on SiN_x and SiO_2, respectively, and sample C is a reference all-PECVD TFT with SiN_x as the gate insulator.

ever, in many cases the high defect density at the grain boundaries and the sensitivity of the Fermi-level position to oxygen contamination by inter-grain diffusion form serious bottlenecks. In high temperature deposition processes, a large grain size is necessary in order to minimize adverse grain boundary defects. In HWCVD, however, due to the lower processing temperature, the grain boundaries remain passivated during deposition, which eliminates the need for post-deposition hydrogen passivation treatments.

The transfer characteristics of three different TFTs are shown in Fig. 7. All three were deposited on thermally grown silicon oxide. The continuous curves are the initial characteristics and the dashed curves are those taken after 23 hours of gate voltage stressing. The top graph is for a typical TFT with a PECVD *a*-Si:H layer (deposition rate 1.5 Å/s), The middle graph is for a TFT that has an HW-deposited *a*-Si:H channel layer made from pure SiH_4 at a deposition rate of 17 Å/s. The bottom graph is for a TFT that has an heterogeneous HW-deposited channel region (deposited under *Poly2-type* conditions, though at slightly higher wire temperature). This resulted in a nucleation layer containing cone shaped crystals, some of which start

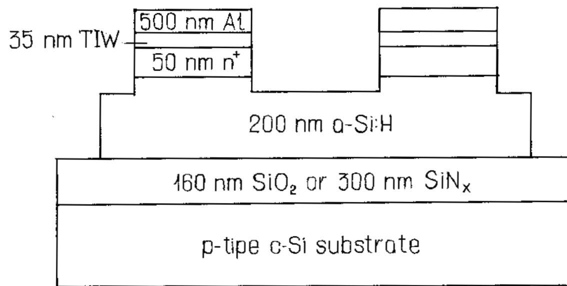

Fig. 6. Sample.

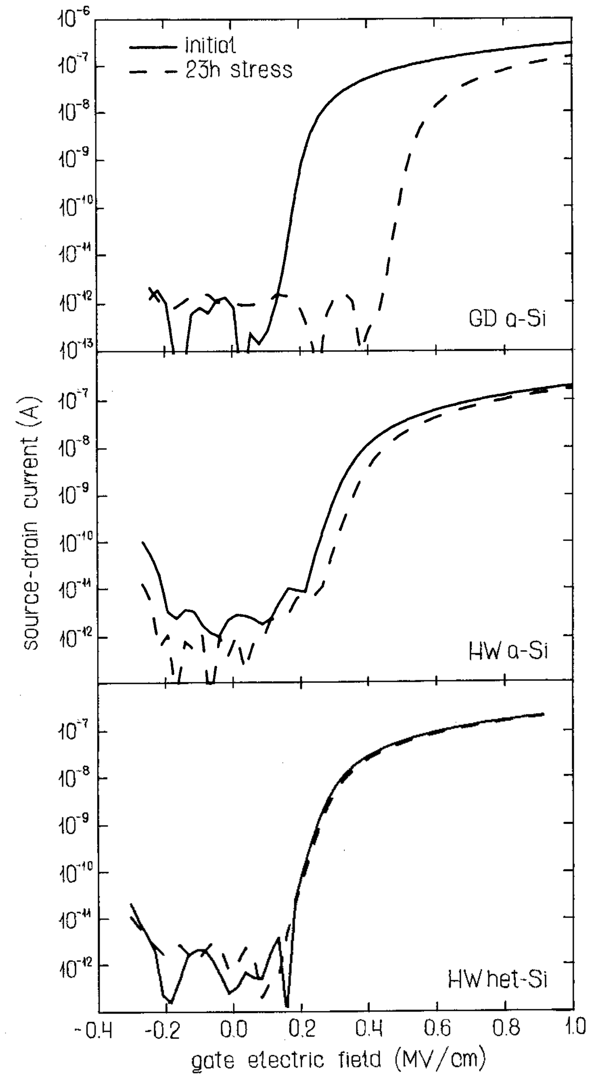

Fig. 7. Linear regime transfer characteristics of poly-Si TFTs with a *a*-Si:H TFTs. All TFTs have HW-deposited active layers. The dashed curves are the characteristics after 23 hours of continuous gate-voltage stress at 1.2 MV/cm.

directly at the insulator interface, leading to a field-effect mobility of 1.1 $cm^2V^{-1}s^{-1}$. For a sample made at *Poly2* conditions (not shown), the usual amorphous incubation layer was present, after which fully coalescent poly-Si growth occurs. The deposition rate of this layer is still high, 8-9 Å/s. Although for these conditions the field-effect channel is located completely within the incubation layer, the mobility is the highest for this TFT, at 1.5 $cm^2V^{-1}s^{-1}$ [28]. This is attributed to the presence of nanocrystalline domains within the largely amorphous matrix of the incubation layer. These domains are only visible in high resolution TEM (HRTEM). Further evidence of the heterogeneous nature of this silicon film is the fact that the electrical characteristics show an inverse Meyer-Neldel relationship [29].

Fig. 7 also shows the transfer characteristics taken after 23 hours of gate voltage stressing at 1.2 MV/cm. It is clearly seen that, whereas the reference TFT shows a considerable threshold voltage shift (ΔV_{th} = 6.2 V), the two HWCVD devices are much more stable. The TFT with the amorphous channel displays a shift of only 0.9 V, whereas the TFT with the heterogeneous channel shows virtually no shift (0.2 ± 0.2 V).

4. SOLAR CELLS

4.1 HW deposited *a*-Si:H *n-i-p* cells

In order to investigate the suitability of Hot-Wire deposited intrinsic amorphous silicon as well as polycrystalline silicon for application in a solar cell these layers were incorporated as the *i*-layer in *n-i-p* structures. Stainless steel served simultaneously as the substrate and as the back metal electrode. First, a thermally stable *n*-type layer was deposited by PECVD [30]. Then the intrinsic HW *a*-Si:H or poly-Si:H was deposited, followed by a wide bandgap buffer layer (2.5 nm thick) and a microcrystalline *p*-type layer. The latter two were again deposited by PECVD. The purpose of the buffer layer between the HW *i*-layer and the μ*c*-Si:H *p*-layer is to prevent back diffusion of electrons generated in the front region. A transparent top window contact was made by reactive evaporation of indium tin oxide (ITO), and had an optical transmission of 90 % and a sheet resistance of 100 Ω/cm. No grid contact was used and the size of the cell was 0.16 cm^2. It should be noted that the efficiency of 5.5 % has been achieved without light-trapping or back-reflection enhancement.

4.2 HW deposited poly-Si:H *n-i-p* cells

In order to test the performance of intrinsic HW-deposited poly-Si layers as the active material in a solar cell, devices were made on an heavily doped *n*-type *c*-Si wafer, which acts as a substrate as well as the *n*-type region. Closer to practical applications, cells were also made on stainless steel (SS) substrates in the configuration SS/*n* μ*c*-Si:H (PECVD)/poly-Si:H (HWCVD)/*p* μ*c*-Si:H (PECVD)/ITO. The *n*- and *p*-type layers were made by PECVD. The cell structures are

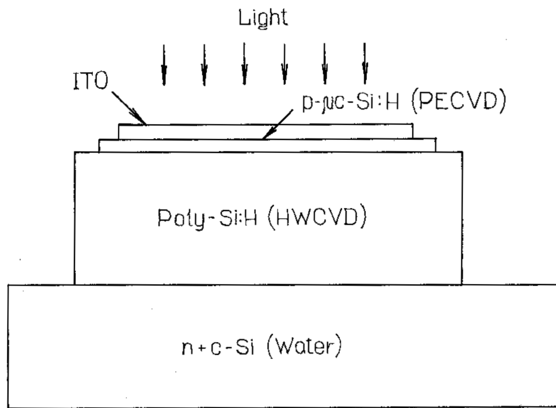

Fig. 8. Cross section view of a test cell on c-Si substrate.

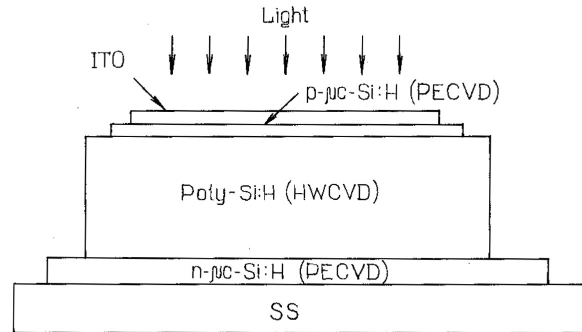

Fig. 9. Cross section view of a test cell on stainless stell substrate.

shown in Figs. 8 and 9, respectively. Representative cell characteristics are shown in Fig. 10.

On *c*-Si, due to the crystallinity of the substrate, *Poly2* conditions lead to immediate nucleation along with typical columnar orientation throughout the bulk. Cells made in this configuration show good characteristics. An unoptimized cell readily shows an efficiency of 3.15 % (Fig. 10a).

When the same *Poly2* conditions are used in the cell configuration using stainless steel with a thin *n*-type μ*c*-Si:H as the substrate instead of an n-type wafer, the cell reaches an efficiency of only 0.64 %, primarily due to a very high series resistance (Fig. 10b). Apparently, layers that are entirely made in the *Poly2* regime can not be used on these substrates, as they have too long an incubation phase. The incubation phase exists because the *n*-type PECVD microcrystalline layer typically has only a small crystalline volume fraction. Therefore, we used a poly-Si:H layer made by implementation of a profiled deposition scheme, as discussed in section 2.3.1. The initial layer is made at high hydrogen dilution on top of which the *Poly2* is grown. In this manner, the incubation layer is avoided. Upon implementation of the interface profiled layer the cell efficiency immediately went to 3.7 % (Fig. 10c).

Upon further optimization, the efficiency could be increased to 4.41 %. No post-deposition hydrogen passivation treatments have been employed. The deposition rate is 5-6 Å/s for the bulk of the intrinsic layer. Fig. 11 shows the cell characteristics. A remarkably high active-area short circuit current density of almost 20 mA/cm^2 (measured with the mask) was achieved for the cell with an active semiconductor film that is only 1.22 μm thick. This value has been verified by convolution of spectral response measurements with the solar irradiation spectrum. In Fig. 12 we show the external collection efficiency of the same cell and of a similar thin film poly-Si cell, which was made thicker. The integrated current density for the 1.22 μm thick cell was 19.36 mA/cm^2, measured under short circuit conditions. This value is within 3 % of the current measured using a solar simulator and thus confirms the current capability of this type of cell. The external collection efficiency of the thicker cell (1.63 μm) in this figure shows the potential for obtaining even higher J_{sc}. The high current generating capability is possible due to the natively textured surface (as observed also in Atomic Force Microscopy), and the high absorption within the film due to internal scattering [31].

It is noted that the V_{oc} is rather low for this cell. We believe that this is due to recombination, in particular at the *n/i* interface region of the cell. The main indication for this is that the V_{oc} is much higher when a heavily doped *n*-type *c*-Si wafer is used as a substrate, serving as the *n*-layer of the cell (Fig. 8). The V_{oc} in that case is 0.454 V rather than 0.365 V as is presently the case. A higher V_{oc} is obtained for the cell with the *n*-layer consisting of a single-crystal wafer, because this cell does not necessitate a profiled seed layer for polycrystalline growth.

The present result compares favorably with recently published results on microcrystalline *n-i-p* cells with efficiencies over 5 % obtained using PECVD, especially considering that (i) our cells do not benefit from much back reflection, as they are made on plain stainless steel serving as the back contact and as they possess an *n*-layer that is made rather thick to avoid metal diffusion into the *i*-layer, and (ii) the deposition rate is 5 - 6 Å/s. The Kaneka group [32] obtained an even higher efficiency of 10.1 % for a cell of 2 μm thickness with a sophisticated back reflector. The deposition rate for these layers has not been published.

5. CONCLUSION

We have demonstrated the potential of the HWCVD technology to produce cheap, thin, and stable thin film

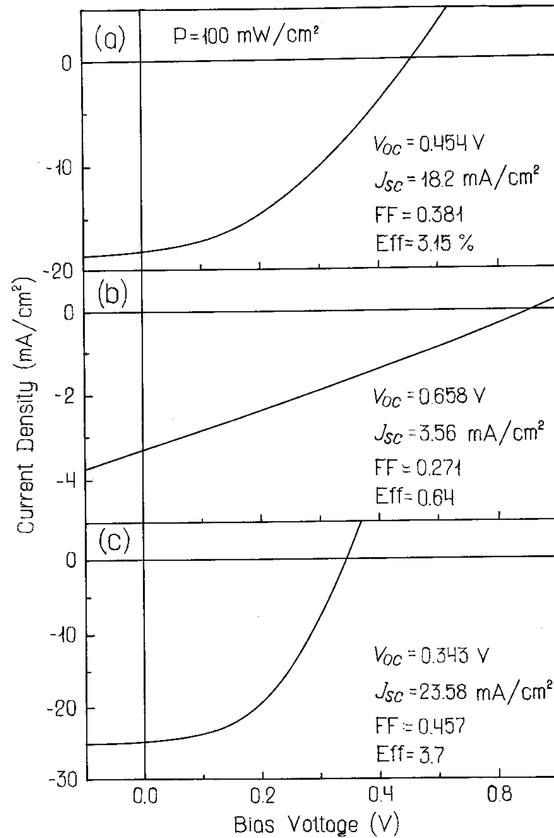

Fig. 10. J-V characteristics taken under 100 mW/cm² AM1.5 illumination of three cells. Graph a) is for a cell in a configuration as in Fig. 8; graph b) is for a cell in a configuration as in Fig. 9; graph c) is for a cell in the same configuration, howerver with a profiled poly-Si:H (*Poly1/Poly2*) i-layer.

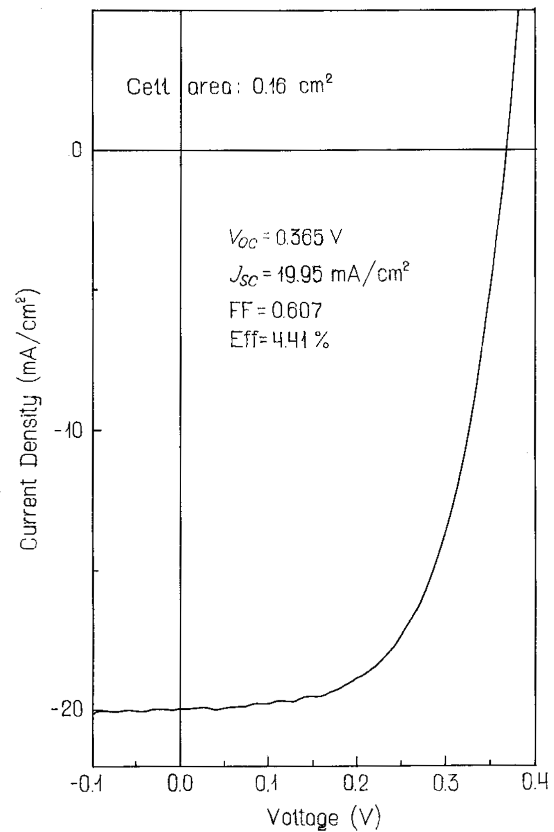

Fig. 11. J-V characteristics under 100 mW/cm² AM1.5 global illumination of *n-i-p* cell with Hot Wire CVD poly-Si:H *i*-layer.

silicon solar cells and thin film transistors on foreign substrates.

The thin film transistors, with the active layer deposited either in an amorphous regime or in a poly-Si regime, show remarkable stability. The highest field-effect mobility (of 1.5 $cm^2V^{-1}s^{-1}$) in an inverted staggered configuration is obtained in a channel, that is in fact an incubation layer made at low hydrogen dilution (*Poly2* conditions). Hot Wire deposited layers can be compatible with plasma-deposited layers as has been demonstrated by the application of PECVD silicon nitride (*a*-SiN_x) as the gate insulator. Thus it is feasible to produce TFTs incorporating Hot-Wire deposited material also on glass substrates, which is important for practical applications.

The thin film *n-i-p* amorphous silicon solar cells an plain stainless steel show an efficiency of 5.5 %. The *n-i-p* polycrystalline silicon cells show a remarkable performance with an active-area efficiency of 4.41 % for a thin cell of only 1.22 μm thickness. Summarizing, it has been shown that HWCVD is a suitable deposition technique for preparing various devices with a performance that can be superior to devices made with conventional PECVD.

ACKNOWLEDGEMENTS

This work was financially supported by the Netherlands Agency for Energy and Environment (NOVEM). We gratefully acknowledge C.H.M. van der Werf and Z. Hartman for numerous sample preparations, and A. Brockhoff for the determination of the first stability results. We are thankful to H. Meiling, who is currently with ASML, Veldhoven, for his effort during the start

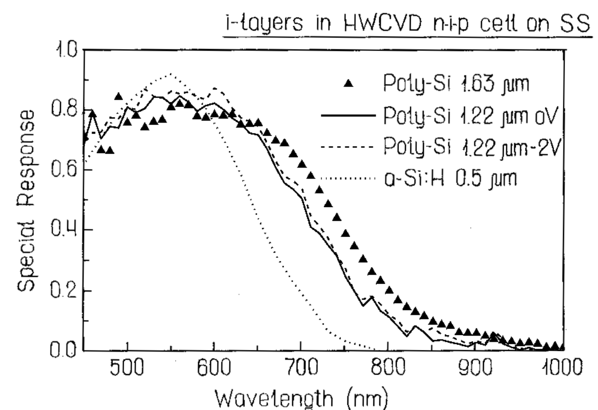

Fig. 12. External spectral collection efficiency characteristics of the *n-i-p* cell with different thicknesses of the *i*-layer. The cells are made without back reflector on plain stainless steel.

up of the TFT research at Utrecht University. We thank J. Holleman and M.H.H. Weusthof of the MESA Research Institute, University of Twente for their assistance in TFT preparation, W. Beyer of the FZ Jiilich for hydrogen evolution experiments, F.D. Tichelaar of TU Delft for TEM work, P. Alkemade of TU Delft for SIMS determinations.

REFERENCES

[I] H. Matsumura // *Jpn. J. Appl. Phys.* **25** (1986) L949.

[2] A.H. Mahan, J. Carapella, B.P. Nelson, R.S. Crandall and I. Balberg // *J. Appl. Phys.* **69** (1991) 6728.

[3] R.E.I. Schropp and M. Zeman, *Amorphous and Microcrystalline Silicon Solar Cells: Modeling, Materials, and Device Technology,* (Kluwer Academic Publishers, Boston-Dordrecht-London, 1998).

[4] R.E.I. Schropp, K.F. Feenstra, E.G. Molenbroek, H. Meiling and J.K. Rath // *Phil. Mag. B* **76** (1997) 309.

[5] H. Wiesmann, A.K. Ghosh, T. McMahon and M. Strongin // *J. Appl. Phys.* **50** (1979) 3752; H.J. Wiesmann: US patent 4,237,150; Dec. 2, 1980.

[6] J. Doyle, R. Robertson, G.H. Lin, M.Z. He and A. Gallagher // *J. Appl. Phys.* **64** (1988) 3215.

[7] H. Matsumura // *Materials Research Society Symp. Proc.* **118** (1988) 43.

[8] H. Matsumura // *J. Appl. Phys.* **65** (1989) 4396.

[9] A.H. Mahan, B.P. Nelson, S. Salamon and R.S. Grandall // *J. Non-Cryst. Solids* **137** & **138** (1991) 657.

[10] A. Madan, P. Rava, R.E.I. Schropp, and B. von Roedern // *Appl. Surf. Sci.***70/71** (1993) 716.

[11] N.H. Nickel, N.M. Johnson and Chris G. van de Walle // *Phys. Rev. Lett.* **72** (1994) 3393.

[12] N.H. Nickel, W.B. Jackson and N.M. Johnson // *Phys. Rev. Lett.* **71** (1993) 2733.

[13] S. Acco, D.L. Williamson, W.G.J.H.M. van Sark, W.C. Sinke, W.F. van der Weg, A. Polman and S. Roorda // *Phys. Rev. B* **58** (1998) 12853.

[14] J.K. Rath, F.D. Tichelaar, H. Meiling, R.E.I. Schropp, In: *Amorphous and Microcrystalline Silicon Technology - 1998*, ed. by R.E.I. Schropp, H. Branz, S. Wagner, M. Hack and I. Shimizu, *Mat. Res. Soc. Symp. Proc.* **507** (1998) 879.

[15] J.K. Rath, H. Meiling and R.E.I. Schropp // *Jpn. J. Appl. Phys.* **36** (1997) 5436.

[16] U. Kroll et al. // *J. Appl. Phys.* **80** (1996) 4971.

[17] J.K. Rath, P. Alkemade and R.E.I. Schropp, *Solar Energy Material and Solar Cells* (in print).

[18] T. Saitoh and H. Hiraki // *Jpn. J. Appl. Phys.* **24** (1985) L491.

[19] D. Stryahilev, F. Diehl and B. Schroeder, *ICAMS18* (Snowbird, USA, 1999) (in print).

[20] J.K. Rath, W. Beyer and R.E.I. Schropp, *ICAMS18*, (Snowbird, USA, 1999), (in print).

[21] J. Meier, P. Torres, R. Platz, S. Dubail, U. Kroll, J.A. Anna Selvan, N. Pellaton Vaucher, Ch. Hof, D. Fischer, H. Keppner, A. Shah, K.-D. Ufert, P. Giannoules and J. Koehler // *Materials Research Society Symp. Proc.* **420** (1996) 3.

[22] J.K. Rath, R.E.I. Schropp and W. Beyer, In: *Proceedings of the 18th International Conference on Amorphous and Micro crystalline Semiconductors,* (Salt Lake City, Utah, Aug. 1999), to be published.

[23] J.K. Rath, F.D. Tichelaar, H. Meiling and R.E.I. Schropp // *Materials Research Society Symp. Proc,* **507** (1998) 879.

[24] J.K. Rath, F.D. Tichelaar and R.E.I. Schropp // *Materials Research Society Symp. Proc.* **557** (1999) to be published.

[25] H. Meiling and R.E.I. Schropp // *Appl. Phys. Lett.* **70** (1997) 2681.

[26] H. Matsumura // *The Electrochem. Soc. Proceedings* **98-22** (1998) 280.

[27] V. Chu, J. Jarego, H. Silva, T. Silva, M. Reissner, P. Brogueira and J.P. Conde // *Appl. Phys. Lett.* **70** (1997) 2741.

[28] H. Meiling, A.M. Brockhoff, J.K. Rath and R.E.I. Schropp // *Materials Research Society Symp. Proc.* **507** (1998) 31.

[29] H. Meiling and R.E.I. Schropp // *Appl. Phys. Lett.* **74** (1999) 1012.

[30] K.F. Feenstra, J.K. Rath, C.H.M. van der Werf, Z. Hartman, and R.E.I. Schropp, In: *Proc. 2nd World Conference and Exhibition on Photovoltaic Solar Energy Conversion (*Vienna, Austria, July 6-10, 199).

[31] Vaněček, Poruba, Remeš, Beck, and Nesládek // *J. Non-Cryst. Solids* **227-230** (1997) 967.

[32] K. Yamamoto // *Materials Research Society Symp. Proc.* **507** (1998) 131.